Eur. Phys. J. B (2012) 85: 322
DOI: 10.1140/epjb/e2012-30121-4

THE EUROPEAN PHYSICAL JOURNAL B

Regular Article

Effects of plasmon pole models on the G^0W^0 electronic structure of various oxides

A. Miglio[1,a], D. Waroquiers[1], G. Antonius[2], M. Giantomassi[1], M. Stankovski[1], M. Côté[2], X. Gonze[1], and G.-M. Rignanese[1]

[1] Institute of Condensed Matter and Nanosciences, Université catholique de Louvain, Chemin des Étoiles 8, bte L7.03.01, 1348 Louvain-la-Neuve, Belgium
[2] Département de physique, Université de Montréal, C.P. 6128, Succursale Centre-Ville, H3C 3J7 Montréal, Canada

Received 9 February 2012
Published online 24 September 2012 –

Abstract. The electronic properties of three different oxides (ZnO, SnO_2 and SiO_2) are investigated within many-body perturbation theory in the G^0W^0 approximation. The frequency dependence of the dielectric function is either approximated using two different well-established plasmon-pole models (one of which enforces the fulfillment of the f-sum rule) or treated explicitly by means of the contour-deformation approach. Comparing these results, it is found that the plasmon-pole model enforcing the f-sum rule gives less accurate results for all three oxides. The calculated electronic properties are also compared with the available experimental data and previous ab initio results, focusing on the d state binding energies. The G^0W^0 approach leads to significantly improved band gaps with respect to calculations based on the density functional theory in the local density approximation.

1 Introduction

While density functional theory (DFT) has proved to be successful in predicting the ground state properties of semiconductors and insulators, the corresponding predicted band gaps are systematically underestimated compared to the experimental values. In fact, DFT is a ground state theory and formally Kohn-Sham (KS) eigenvalues cannot be interpreted as quasiparticles (QP) energies.

In contrast, many-body perturbation theory (MBPT) allows one to determine the excited-state properties (e.g. single-particle addition and removal energies) and therefore the QP band structures with very good accuracy. The key quantity in MBPT is the self-energy operator Σ which carries information related to the many-body interactions between the particles. It is non-local, non-Hermitian and energy dependent. In fact, the main difficulty is to find an adequate expression for Σ. Hedin [1] proposed a perturbative approach in which the self-energy operator is obtained by solving self-consistently a set of coupled integro-differential equations. This scheme being very cumbersome, Hedin also suggested an approximation for the vertex function Γ which appears in these equations. As a result, the self-energy operator is simply obtained as the product of the Green's function (G) and the dynamically screened Coulomb potential (W). In principle, the self-consistency requirement still holds. However, it is customary to stop after the first iteration, which is often referred to as one-shot GW or G^0W^0. In this framework, the self-energy operator is obtained from the KS states. The G^0W^0 method usually leads to very reasonable band gaps and bandstructures for quite a large range of semiconducting and insulating materials.

In practice, it is most efficient to obtain the QP energies using perturbation theory with respect to the results of DFT: the self-energy operator Σ is treated as a correction to the exchange-correlation potential of the system in the KS picture. The QP energies are thus computed by adding QP corrections to the KS eigenvalues. This procedure will result in values in agreement with experiment provided that the KS states are similar to the QP states. Otherwise a self-consistent approach on the eigenvalues, and possibly on the eigenstates, might be necessary. Recently, it was shown that G^0W^0 results may depend not only on the KS starting point but also on a subsequent approximation in the treatment of the frequency dependence of the dielectric function [2]: namely the use of plasmon pole models (PPMs) [3]. Analyzing the differences between different PPMs is important in the evaluation of the G^0W^0 approximation and its reliability. That is the aim of the present paper.

We focus on three different oxides (ZnO, SnO_2 and SiO_2) and we compare the effects of DFT in the local density approximation (LDA) and standard GW approximations of the dielectric function on their fundamental band gap and the semicore d state binding energies. We then compare our results to available experimental data and discuss in further detail the electronic structure.

First-principles electronic structure calculations on these oxides have already been carried out with different methods, most of them within the framework of DFT.

[a] e-mail: anna.miglio@uclouvain.be

More recently, MBPT was used to better describe excited-state properties, mainly the band gap [4–22], but there are still significant discrepancies up to the order of 1 eV in the reported band gap values.

This work is organized as follows: we first describe the theoretical methods; we then discuss the results for ZnO, SnO_2 and SiO_2 and compare them to available experimental data and previously reported abinitio results.

2 Theoretical methods

If KS orbitals are a good approximation to the pertubatively corrected QP orbitals then only one iteration of Hedin's GW approximation [1] needs to be performed i.e. the so-called G^0W^0 approach.

The Green's function G and the screened Coulomb potential W are needed to compute Σ:

$$\Sigma(r,r';\omega) = \frac{i}{2\pi}\int_{-\infty}^{\infty} d\omega' G(r,r';\omega+\omega')W(r,r';\omega')e^{i\omega'\eta}, \tag{1}$$

G is represented in terms of the KS orbitals ϕ_i and energies ε_i^{KS}as

$$G(r,r';\omega) = \sum_i \frac{\phi_i^*(r')\phi_i(r)}{\omega-\varepsilon_i^{KS}-i\eta}, \tag{2}$$

where $\eta = 0^+$ for occupied states i.e. hole excitations and $\eta = 0^-$ for unoccupied states i.e. electronic excitations. The dynamically screened Coulomb potential is given by

$$W(r,r';\omega) = \int dr'' \epsilon^{-1}(r,r'';\omega)v(r'',r'), \tag{3}$$

where $v(r,r')$ is the bare Coulomb potential and $\epsilon(\mathrm{r},\mathrm{r}';\omega)$ is the dielectric function. The self-energy is usually separated into a frequency independent pure-exchange part Σ_x and a correlation part Σ_c to give $\Sigma(\omega) = \Sigma_\mathrm{x} + \Sigma_\mathrm{c}(\omega)$, where:

$$\Sigma_\mathrm{x} = \frac{i}{2\pi}\int_{-\infty}^{\infty} d\omega' G(\omega')v e^{i\omega'\eta}, \tag{4}$$

and

$$\Sigma_\mathrm{c}(\omega) = \frac{i}{2\pi}\int_{-\infty}^{\infty} d\omega' G(\omega+\omega')[W(\omega')-v]. \tag{5}$$

We have omitted the spatial part in the previous equations for Σ, since it is a pure multiplication. The quasiparticle energies are then obtained perturbatively, assuming ε_i^{QP} close to ε_i^{KS}

$$\varepsilon_i^{QP} = \varepsilon_i^{KS} + Z_i \left\langle \phi_i^{KS} | \Sigma(r,r';\varepsilon_i^{KS}) - V_{xc}(r)\delta(r-r') | \phi_i^{KS} \right\rangle \tag{6}$$

where Z_i is the renormalization factor

$$Z_i^{-1} = 1 - \left\langle \phi_i^{KS} \right| \left.\frac{\partial\Sigma(\omega)}{\partial\omega}\right|_{\varepsilon_i^{KS}} \left| \phi_i^{KS} \right\rangle. \tag{7}$$

PPMs are used to compute Σ_c by approximating the convolution integral (5). In a periodic system, where ϵ^{-1} is the inverse dielectric matrix in the random phase approximation (RPA) [23,24], the dynamical part of the screened interaction defined as $W^\mathrm{c} = W - v$ reads

$$W^\mathrm{c}_{\mathbf{G},\mathbf{G}''}(\mathbf{q},\omega) = \sum_{\mathbf{G}'}[\epsilon^{-1}_{\mathbf{G},\mathbf{G}'}(\mathbf{q},\omega) - \delta_{\mathbf{G},\mathbf{G}'}]v_{\mathbf{G}',\mathbf{G}''}(\mathbf{q}), \tag{8}$$

with $\mathbf{G}$ and $\mathbf{q}$ being the reciprocal lattice vectors and wave vectors within the first Brillouin zone (BZ) respectively. The frequency dependence of the imaginary part of W^c i.e. ϵ^{-1} is assumed to be well described by a delta peak function, which introduces three parameters: the weight of the peak, A, the pole frequency $\tilde{\omega}$, and the oscillator strength of the real part, Ω:

$$\begin{aligned}\Im[\epsilon^{-1}_{\mathbf{G},\mathbf{G}'}(\mathbf{q},\omega)] &= A_{\mathbf{G},\mathbf{G}'}(\mathbf{q}) \\ &\quad\times[\delta(\omega-\tilde{\omega}_{\mathbf{G},\mathbf{G}'}(\mathbf{q})) - \delta(\omega+\tilde{\omega}_{\mathbf{G},\mathbf{G}'}(\mathbf{q}))], \\ \Re[\epsilon^{-1}_{\mathbf{G},\mathbf{G}'}(\mathbf{q},\omega)] &= \delta_{\mathbf{G},\mathbf{G}'} + \frac{\Omega^2_{\mathbf{G},\mathbf{G}'}(\mathbf{q})}{\omega^2-\tilde{\omega}^2_{\mathbf{G},\mathbf{G}'}(\mathbf{q})}.\end{aligned} \tag{9}$$

Kramers-Kronig relations apply to W and therefore only two parameters are independent.

In this work, we use the PPMs introduced by Hybertsen and Louie (HL) [25] and Godby and Needs (GN) [26]. Both PPMs set the plasmon pole parameters first requiring that the behavior of ϵ^{-1} in the static limit ($\omega = 0^+$) is reproduced. In the HL PPM, the parameters are chosen so that the dielectric function fulfills a frequency sum rule (f-sum rule) [27]:

$$\int_0^\infty d\omega\,\omega\Im[\epsilon^{-1}_{\mathbf{G},\mathbf{G}'}(\mathbf{q},\omega)] = -\frac{\pi}{2}\omega_p^2\frac{(\mathbf{q}+\mathbf{G})\cdot(\mathbf{q}+\mathbf{G}')}{|\mathbf{q}+\mathbf{G}|^2}\frac{n_{\mathbf{G}-\mathbf{G}'}}{n_{\mathbf{G}=\mathbf{0}}}, \tag{10}$$

where $n_{\mathbf{G}-\mathbf{G}'}$ is the charge density in reciprocal space. In the GN PPM, the parameters are determined by computing the value of ϵ^{-1} at one point on the imaginary frequency axis $i\omega_p$ near the plasma frequency of the system.

One can avoid using a PPM by doing a full-frequency treatment of the convolution in equation (5) (see Ref. [28,29]). Although computationally expensive, it allows for a more accurate description of Σ_c. The contour deformation technique (CD) eases this treatment by deforming the integration path. The correlation Σ_c is then computed as the difference between an integral along the imaginary axis and the contribution due to the residues of the poles of G inside the contour.

$$\begin{aligned}\Sigma_c(\omega) = &-\sum_s^{\mathcal{C}}\lim_{z\to z_s} G(z)W^\mathrm{c}(z)(z-z_s) \\ &-\frac{i}{2\pi}\int_{+\infty}^{-\infty} d(i\omega')G(\omega+i\omega')W^\mathrm{c}(i\omega'),\end{aligned} \tag{11}$$

where $z_s = \epsilon_s^{KS} - \omega + i\eta$ and the appropriate sign of the residues has to be taken into account. In Figure 1 we illustrate the contour $\mathcal{C}$ in the complex plane used to compute the integral in equation (5).

3 Computational details

All calculations are performed with the ABINIT code [30] which relies on a plane wave approach. The electron-ion

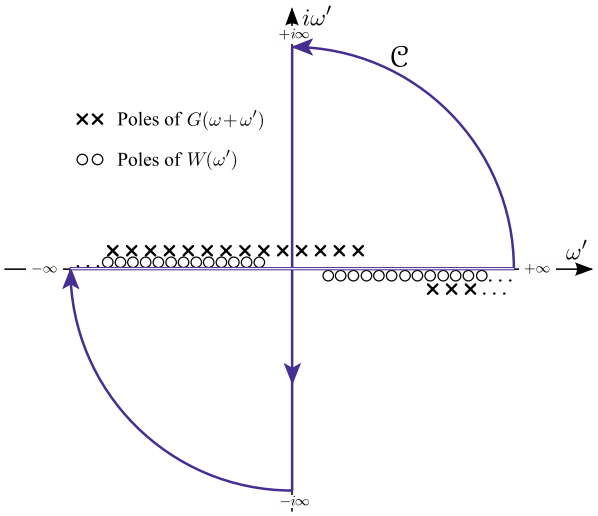

Fig. 1. (Color online) The contour integration path (blue line) for the frequency integration of equation (5) in the complex plane. The integration along the real frequency axis is changed into an integration along the imaginary axis plus summation of the enclosed poles.

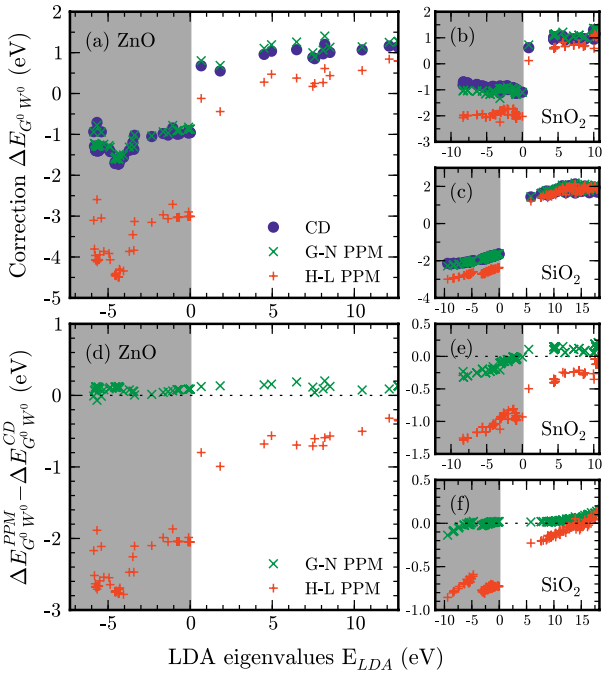

Fig. 2. (Color online) Upper panel: QP corrections with respect to LDA energies in the gap energy range, computed for a sampling of points in the BZ. Data were obtained with the contour deformation technique (blue circles), Godby-Needs PPM (green crosses) and Hybertsen-Louie PPM (red plus), respectively for ZnO (a), SnO_2 (b) and SiO_2 (c). The shaded regions correspond to occupied states. Lower panel: the error of Godby-Needs and Hybertsen-Louie PPMs with respect to the full-frequency contour deformation technique, for ZnO (d), SnO_2 (e) and SiO_2 (f).

interaction is modeled by standard norm-conserving pseudopotentials [31] including scalar relativistic corrections for Zn and Sn ions. Zn and Sn semicore d states are treated as valence electrons as well as the complete shell to which they belong. Indeed, it has been previously shown [32] that all the electron states in shell with semicore d states need to be included in order to get accurate QP energies. In all calculations, the exchange-correlation energy is described using an LDA functional [33]. For all three oxides, the calculations are performed at experimental structural parameters and in the frozen lattice approximation, neglecting electron-phonon interactions effects. The cut-off energies for the wavefunctions and the dielectric matrix, as well as the number of empty states included in the calculations of W and Σ are set to converge the eigenenergies within 0.05 eV.

For ZnO, the wurtzite phase (space group $P6_3mc$) is considered. The experimental data from reference [34] are used for the structural parameters ($a = b = 3.25$ Å, $c = 5.20$ Å, and $u = 0.382$). The pseudopotentials are generated using the following electronic valence configurations: $3s^2\ 3p^6\ 3d^{10}\ 4s^2$ electrons for Zn and $2s^2\ 2p^4$ for O. A $5 \times 5 \times 4$ Monkhorst-Pack (MP) [35] grid is used to sample the BZ. The grid is shifted by $(0, 0, \frac{1}{2})$ (reduced coordinates) for the calculation of W, and Γ centered in the calculation of Σ.

SnO_2 crystallizes in the rutile structure (space-group symmetry $P4_2/mnm$). The tetragonal Bravais lattice contains two formula units per primitive cell with the oxygen atoms forming a distorted octahedron around the tin atom. The experimental structural parameters ($a = 3.18$ Å, $c = 4.74$ Å, and $u = 0.307$) are those reported in reference [36]. In the pseudopotentials generation, the Sn $5p^2$, $5s^2$, $4d^{10}$, $4p^6$, $4s^2$ electrons and O $2s^2$, $2p^4$ electrons were treated as valence states. The calculations are performed on a Γ centered $4 \times 4 \times 6$ MP grid except for the evaluation of W where a $(\frac{1}{2}, \frac{1}{2}, \frac{1}{2})$ shift is applied.

For SiO_2, we consider the α-quartz structure which has hexagonal symmetry (space-group $P3_221$). Its unit cell contains three formula units. The structural parameters are fixed at the experimental value ($a = b = 4.91$ Å, $c = 5.40$ Å, $u = 0.465$, $x = 0.415$, $y = 0.272$, and $z = 0.120$) as reported in reference [37]. We use a Γ centered $2 \times 2 \times 2$ MP grid, while W is computed on a grid shifted by $(0, 0, \frac{1}{2})$.

4 Results and discussion

In Figure 2, we probe the effects of using a PPM approximation looking at G^0W^0 corrections to the LDA eigenvalues for ZnO, SnO_2 and SiO_2. The results computed with GN and HL PPMs are compared to those calculated without resorting to any approximation on the frequency-dependence of the dielectric matrix (i.e. using the CD technique). The results obtained with the GN PPM are in excellent agreement with the CD results, not only for the band gap but also for the absolute values of the G^0W^0 shifts. The latter are critical for band offsets studies [38,39]. The size of the QP corrections to the LDA eigenvalues depends also on the orbital character of the corresponding state. For ZnO and SnO_2, an accurate description of the semicore states (not shown for SnO_2 in Fig. 2) requires the full-frequency approach of the CD

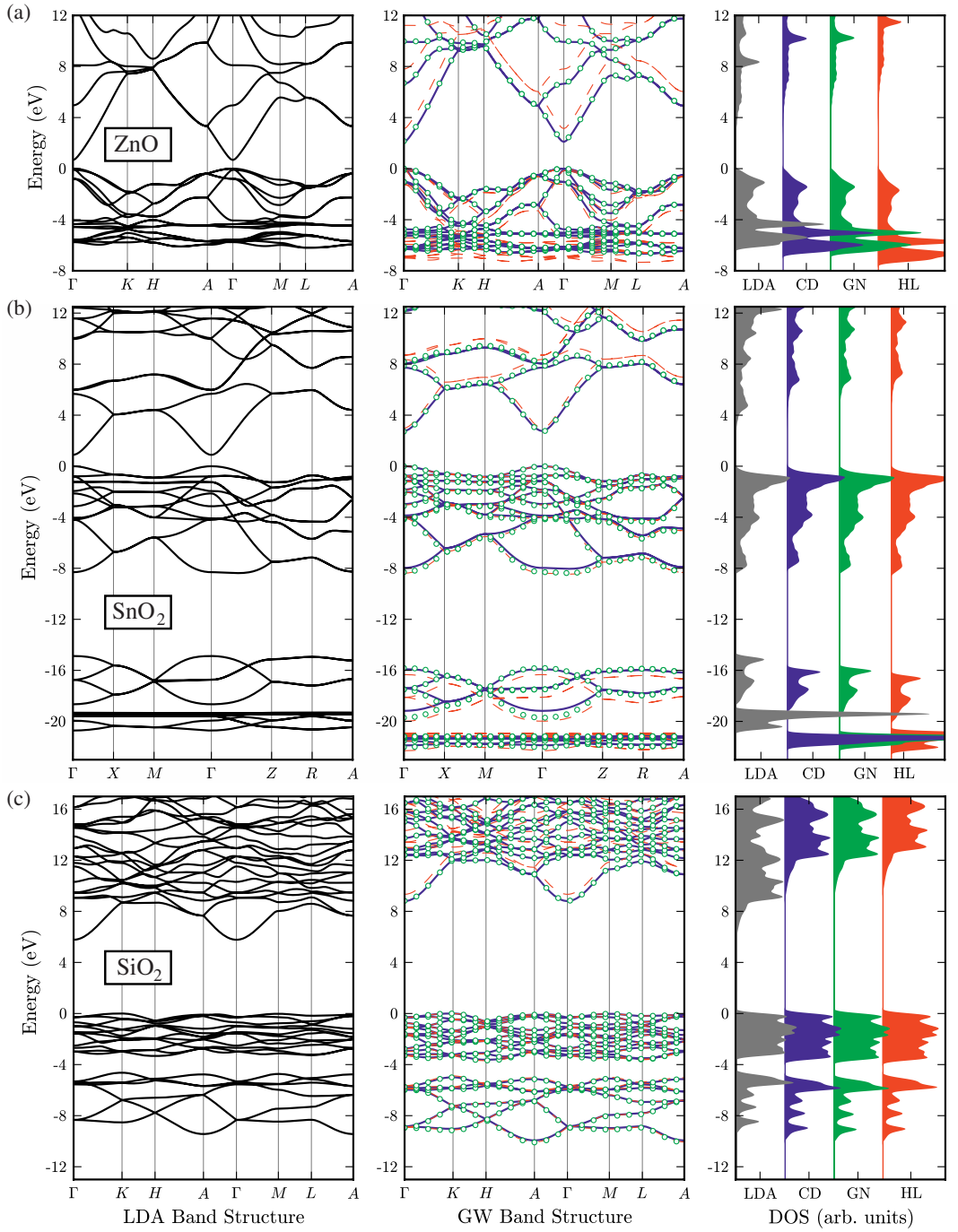

Fig. 3. (Color online) Bandstructures and DOS for ZnO (a), SnO_2 (b) and SiO_2 (c) as computed within LDA (solid black line), the contour deformation technique (solid blue line), Godby-Needs PPM (green circles) and Hybertsen-Louie PPM (dashed red line). In each panel, the top of the valence band has been set to 0.

technique [39] as both PPMs fail to provide a good description of states far from the Fermi level.

In ZnO, the HL PPM strongly overestimates the corrections for all states, especially for those close to the top of the valence band. The effect is an artificial opening of the ZnO gap, as already emphasized in [2]. This overestimation is also present, though smaller, in SnO_2 and SiO_2. For SiO_2, the G^0W^0 corrections to the KS eigenvalues are almost linear and the overall effects on the bandstructure is almost a rigid shift i.e. the use of a scissor operator would be appropriate. A clearer estimate of the precision of the GN PPM with respect to the reference CD is given at the bottom of Figure 2. The GN QP corrections are in very good agreement with the CD results over the whole considered energy range.

The LDA and G^0W^0 bandstructures and density of states (DOS) of ZnO, SnO_2 and SiO_2 are plotted in Figure 3. The G^0W^0 results are obtained using a polynomial

Table 1. Fundamental band gap (in eV) of ZnO, SnO_2 and SiO_2 (indirect for SiO_2 from K^v to Γ^c) computed within LDA and G^0W^0 using the contour deformation (CD) technique, the Godby-Needs (GN) and Hybertsen-Louie (HL) PPMs.

E_g	LDA	CD	GN PPM	HL PPM	exp
ZnO	0.67	2.43	2.34	3.56	3.44[a] 3.6[b]
SnO_2	0.89	2.61	2.72	3.05	3.6[c]
SiO_2	5.77	8.89	8.88	9.36	∼9[d]

[a] Reference [43]. [b] Reference [44]. [c] Reference [45].
[d] References [46,47].

interpolation of the computed QP energies at different points of the BZ. All energies are referenced to the top of the valence band. Experimentally the Zn 3*d* levels lay 7.5–8.8 eV [40] below the top-most valence bands. However, it is apparent by inspection of Figure 3a that not even G^0W^0 calculated in the full-frequency approach is able to assign the correct energies to the ZnO *d* states. We have argued in a previous work [2] that the addition of a Hubbard U term only corrects the QP energies to a limited extent. In wurtzite ZnO the Zn *d* orbitals couple with the O *p* states at the valence band maximum (VBM). As a consequence of the poor description of these states the VBM is pushed upwards and the band gap is then reduced. The band gap value (Tab. 1) is then underestimated by ∼35%. The theoretical estimation of the ZnO band gap has been a very active subject of investigation and debate in the ab initio community. Theoretical band gap values recently published range from 2.1 eV to 3.4 eV [5–14].

In the SnO_2 LDA band structure in Figure 3b, the bands lying in the region located from 19 to 21 eV below the VBM correspond to the Sn 4*d* electrons which are treated as valence electrons. In the XPS experimental density of states spectrum, these bands appear at 21.5–22.5 eV [41,42] below the main peak which is due to O *p* states close to VBM. In all G^0W^0 bandstructures, these bands are shifted down in energy and are thus in better agreement with experiment. As observed in other oxides e.g. ZnO, the well known underestimation of O *p*-Sn *d* repulsion occurs also for SnO_2, although it is smaller due to the deeper position in the VBM of the Sn 4*d* band, with respect to the 3*d* bands of ZnO. The top of the VBM mainly consists of contributions from the O *p* states, while the bottom of the conduction band minimum (CBM) has an anti-bonding character arising from the Sn 4*s* and O *p* states. Our SnO_2 quasiparticle LDA+G_0W_0 results give a direct band gap value range of 2.6–3.1 eV depending on the PPMs, in agreement with recently published theoretical value of 2.88–2.9 eV [17] but underestimating the experimental band gap (3.6 eV) by ∼25–15% (see Tab. 1).

SiO_2 upper valence bands are constituted mainly by O *p* states, while Si 3*s* and 3*p* as well as O 2*s* and 2*p* states hybridize to form the conduction bands. The density of states spectrum (Fig. 3c) compares well with XPS measurements reported in reference [48]. In SiO_2 the computed band gap is in very good agreement with recently published values [21,22] and the error is smaller than 1%.

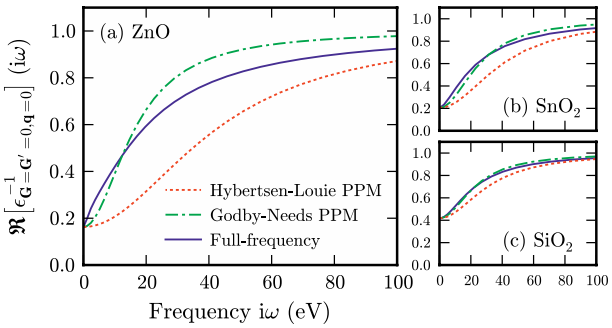

Fig. 4. (Color online) Real component [at $\mathbf{G} = \mathbf{G}' = 0$ and $\mathbf{q} = 0$] of the RPA microscopic dielectric function ϵ^{-1} as computed with the full frequency contour deformation technique (solid blue), the Godby-Needs PPM (dot-dashed green), and the Hybertsen-Louie PPM (dotted red) plotted along the imaginary axis for (a) ZnO, (b) SnO_2, and (c) SiO_2.

Clearly the KS energies and wavefunctions of ZnO and SnO_2 are not a sufficiently accurate starting point for *GW*. More sophisticated and computationally expensive methods might achieve a better accuracy e.g. *GW* self-consistent approximations such as self-consistent COHSEX [3] as a starting point for G^0W^0 [49], quasiparticle self-consistent *GW* à la Kotani-Faleev [8] or including excitonic effects via vertex corrections to the *GW* self-energy.

For all the oxides considered in this work we observe a similar convergence behavior of the band gap value, as the one illustrated in detail in reference [2] for the ZnO case only. The band gap computed within the HL PPM approximation converges slower than with GN PPM and CD, with respect to both the number of unoccupied bands included in the calculation and the planewave cut-off. This feature is less pronounced in SiO_2 and it should be ascribed to the absence of localized semicore states in the electronic density $n_{\mathbf{G}-\mathbf{G}'}$ (see Eq. (10)).

We analyze the properties of the dielectric matrices obtained with the CD technique and with the PPMs to further investigate the reasons leading to the discrepancies we listed above. In Figure 4 the real part of the dielectric matrix $\Re[\epsilon^{-1}(i\omega)]$ along the imaginary frequency axis for $\mathbf{q} = 0$ at $\mathbf{G} = \mathbf{G}' = 0$ computed with the PPMs is compared to the more accurate values obtained with the CD technique. It is clear that the GN PPM better reproduces the CD results. Indeed, the GN PPM parameters are determined from the value of ϵ^{-1} for the static limit ($\omega = 0^+$) and evaluated at one frequency $i\omega_p$ along the imaginary axis, the value of which corresponds to the intersection of the CD and GN curves in Figure 4. In view of this, it is not surprising that the GN PPM reproduces the behavior of the dielectric matrix along the imaginary axis fairly well. In contrast, the HL PPM does not give the correct $\Re[\epsilon^{-1}(i\omega)]$ behavior. In all three cases illustrated in Figures 4a–4c the HL PPM is strongly underestimating the behavior of the CD results over the whole frequency range.

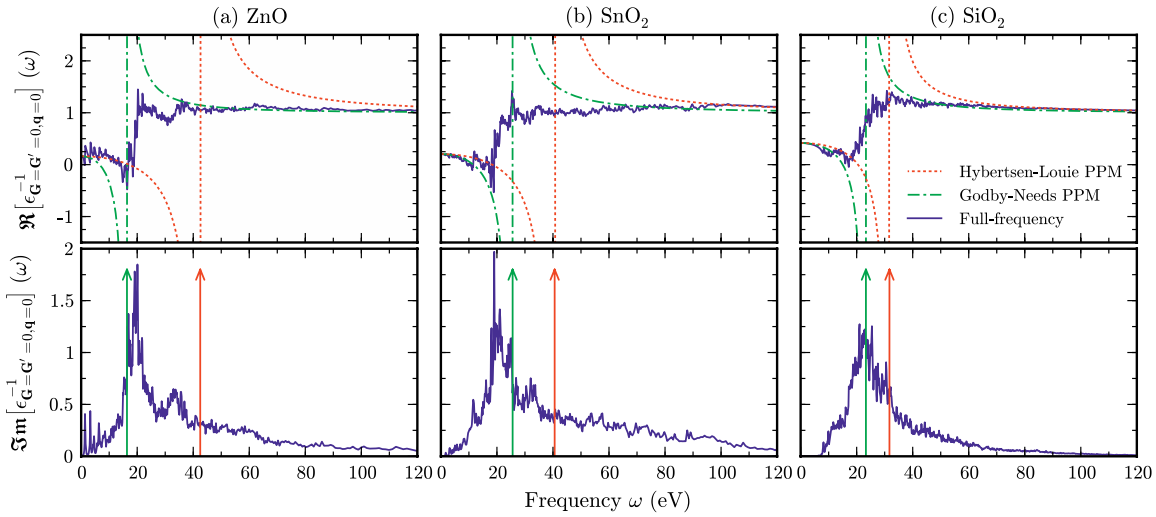

Fig. 5. (Color online) Real (upper panel) and imaginary (lower panel) components (at $\mathbf{G} = \mathbf{G}' = 0$ and $\mathbf{q} = 0$) of the RPA microscopic dielectric function ϵ^{-1} as computed with the contour deformation technique (solid blue), the Godby-Needs PPM (dot-dashed green), and the Hybertsen-Louie PPM (dotted red) plotted along the real axis for (a) ZnO, (b) SnO_2, and (c) SiO_2.

The real part of $\epsilon^{-1}(\omega)$ along the real frequency axis is shown in the upper panel of Figure 5 for $\mathbf{q} = 0$ at $\mathbf{G} = \mathbf{G}' = 0$. By construction, both PPMs match at the static limit $\omega = 0^+$. For all three cases, though the two PPMs are both crude approximations, the GN PPM is closer to the exact behavior of $\Re[\epsilon^{-1}(\omega)]$, in particular for frequencies larger than the position of the main pole. For SnO_2 and SiO_2, the GN PPM is also a much better approximation for very small frequencies (ω <10 eV) while this is not apparent in the ZnO case. These small frequencies correspond to the range needed for the evaluation of the QP corrections to the states close to the band gap.

The imaginary part of ϵ^{-1} is shown in the lower panel of Figure 5. The position of the Dirac delta peaks for the PPMs where all the spectral weight of $\Im[\epsilon^{-1}(\omega)]$ is concentrated is represented by the arrows. For the three systems, the GN pole peak seems to better account for the overall peak structure of $\Im[\epsilon^{-1}(\omega)]$. For higher $\mathbf{G}, \mathbf{G}'$ vectors, the position of the peaks for the GN and HL PPMs is affected in a very different manner. The sum rule imposed by the HL model pushes the Dirac delta peak ever further on the real axis as can be seen in the upper panel of Figure 6. This seems to result in an overestimation of the pole contribution along the imaginary axis, in particular for the low frequency region.

We then considered how the different techniques we used to compute the screening comply with the sum rule. The HL PPM complies with the sum rule by construction, while in the GN PPM, the parameters fix the integral of the imaginary part of the inverse dielectric function. When $\Im[\epsilon^{-1}(\omega)]$ is calculated explicitly, the integral depends on the number of empty states included in the sum. In the lower panels of Figure 6, we show how the fulfillment of the sum rule varies for the diagonal matrix elements of $\Im[\epsilon^{-1}(\omega)]$. The compliance with the sum rule is slowly achieved by the full-frequency CD while for the GN PPM it is rather poor. Although the HL PPM fulfills the sum rule by definition, it leads to some inaccuracies for ϵ^{-1} at low frequencies which we can trace back to its underlying assumptions. We can see from the lower panel of Figure 5 that for ZnO and SnO_2, the absorption spectra indicate that there are many plasmon features probably related to the highly inhomogeneous nature of the charge density in those systems. The HL PPM averages these contribution by enforcing the fulfillment of the f-sum rule to set the position of a single pole. The GN PPM, on the other hand, concentrates the fitting at a specific range by evaluating another dielectric matrix at a non zero frequency. The resulting pole is placed closer to the main feature of the spectrum for the long-wavelength components of the dielectric matrix. This might however not be the case for the short-wavelength components, as was shown in reference [2]. It is therefore expected that the HL PPM might be less suitable for highly inhomogeneous charge densities, or more specifically for systems with localized states, and this is what is observed in the examples presented in this study.

5 Conclusions

In this study, three different oxides have been used as benchmarks to test the accuracy of two PPMs with respect to the more computationally demanding full frequency CD approach. Our results show that the GN PPM approximation systematically gives a reliable estimate – compared to CD calculations – of the band gap values and of the absolute values of the QP energies over a quite wide energy range. In light of our analysis of the PPMs description of ϵ^{-1}, the fulfillment of the sum rule in all the systems under consideration seems not to be a significant and sufficient condition to ensure reliable results. The overall agreement with experimental results is strongly influenced by the presence of the d levels in both ZnO and

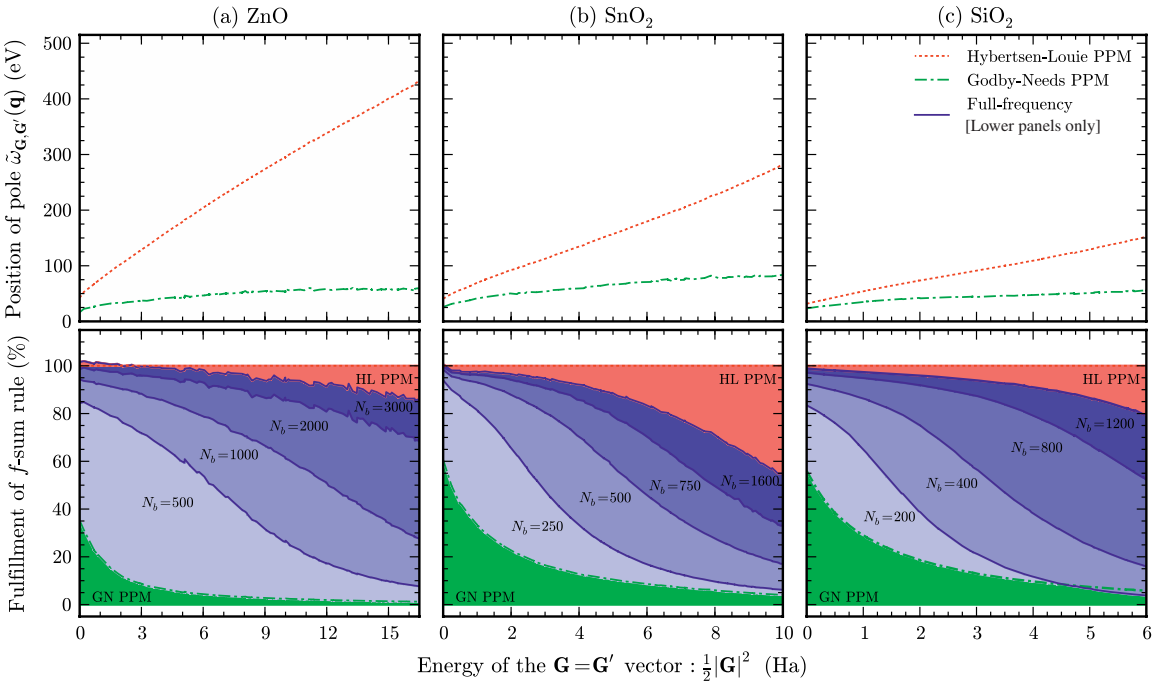

Fig. 6. (Color online) Position of pole (upper panel) and fulfillment of the f-sum rule (lower panel) for the diagonal elements ($\mathbf{G} = \mathbf{G}'$) of ϵ^{-1} within the Godby-Needs (dot-dashed green) and Hybertsen-Louie (dotted red) PPMs as a function of the corresponding kinetic energy ($\frac{1}{2}|\mathbf{G}|^2$). The blue/dark gray curves are the results obtained with the full frequency contour deformation technique when varying the number of unoccupied bands included in the calculation of ϵ^{-1}. The results for (a) ZnO, (b) SnO_2, and (c) SiO_2 are compared. The band gap computed with the contour deformation technique is converged with ∼1250, ∼1000 and ∼400 unoccupied states for ZnO, SnO_2 and SiO_2 respectively.

SnO_2. We can then conclude that the LDA + G^0W^0 approach is not accurate enough to reproduce the electronic features of ZnO and to some extent SnO_2 and thus more sophisticated approaches, such as full self-consistent GW, are needed for these materials.

We would like to acknowledge technical support from Y. Pouillon, A. Jacques and J.-M. Beuken. M.C. and G.A. would like to acknowledge the support of NSERC and FQRNT. A.M. would like to thank A. Berger for discussions about SnO_2. This work was supported by the Interuniversity Attraction Poles program (P6/42) – Belgian State – Belgian Science Policy, the IWT project Number 080023 (ISIMADE), the EU's 7th Framework programme through the ETSF I3 e-Infrastructure project (Grant agreement 211956), the Communauté française de Belgique, through the Action de Recherche Concertée 07/12-003 "Nanosystèmes hybrides métal-organiques", the FRS-FNRS through FRFC project Nos 2.4.589.09.F and 2.4645.08. The Région Wallonne through WALL-ETSF project Number 816849.

References

1. L. Hedin, S. Lundqvist, in *Solid State Physics*, edited by H. Ehrenreich, F. Seitz, D. Turnbull (Academic, New York, 1969), Vol. 23, p. 1
2. M. Stankovski, G. Antonius, D. Waroquiers, A. Miglio, H. Dixit, K. Sankaran, M. Giantomassi, X. Gonze, M. Côté, G.-M. Rignanese, Phys. Rev. B **84**, 241201(R) (2011)
3. L. Hedin, Phys. Rev. A **139**, 796 (1965)
4. S. Massidda, R. Resta, M. Posternak, A. Baldereschi, Phys. Rev. B **52**, R16977 (1995)
5. M. Usuda, N. Hamada, T. Kotani, M. van Schilfgaarde, Phys. Rev. B **66**, 125101 (2002)
6. A.R.H. Preston, B.J. Ruck, L.F.J. Piper, A. De Masi, K.E. Smith, A. Schleife, F. Fuchs, F. Bechstedt, J. Chai, S.M. Durbin, Phys. Rev. B **78**, 155114 (2008)
7. A. Schleife, C. Rödl, F. Fuchs, J. Furthmüller, F. Bechstedt, P.H. Jefferson, T.D. Veal, C.F. McConville, L.F.J. Piper, A. DeMasi, K.E. Smtih, H. Lösch, R. Goldhahn, C. Cobet, J. Zúñiga-Pérez, V. Muñoz-Sanjosé, J. Korean Phys. Soc. **53**, 2811 (2008)
8. T. Kotani, M. van Schilfgaarde, S.V. Faleev, Phys. Rev. B **76**, 165106 (2007)
9. M. Shishkin, G. Kresse, Phys. Rev. B **75**, 235102 (2007)
10. F. Fuchs, J. Furthmüller, F. Bechstedt, M. Shishkin, G. Kresse, Phys. Rev. B **76**, 115109 (2007)
11. P. Gori, M. Rake, C. Cobet, W. Richter, N. Esser, A. Hoffmann, R. Del Sole, A. Cricenti, O. Pulci, Phys. Rev. B **81**, 125207 (2010)
12. H. Dixit, R. Saniz, D. Lamoen, B. Partoens, J. Phys.: Condens. Matter **22**, 125505 (2010)
13. B.-C. Shih, Y. Xue, P. Zhang, M.L. Cohen, S.G. Louie, Phys. Rev. Lett. **105**, 146401 (2010)
14. C. Friedrich, M.C. Müller, S. Blügel, Phys. Rev. B **83**, 081101(R) (2011)
15. M. Palummo, L. Reining, M. Meyer, C.M. Bertoni, in *22nd Intern. Conf. on the Phys. of Semicond.*, edited by D.J. Lockwood (World Scientific, Singapore, 1995)
16. C. Sevik, C. Bulutay, Phys. Rev. B **74**, 193201 (2006)

17. J.A. Berger, L. Reining, F. Sottile, Phys. Rev. B **82**, 041103(R) (2010)
18. R. Saniz, H. Dixit, D. Lamoen, B. Partoens, Appl. Phys. Lett. **97**, 261901 (2010)
19. A. Schleife, M. Eisenacher, C. Rödl, F. Fuchs, J. Furthmüller, F. Bechstedt, Phys. Rev. B **83**, 035116 (2011)
20. E.K. Chang, M. Rohlfing, S.G. Louie, Phys. Rev. Lett. **85**, 2613 (2000)
21. L. Martin-Samos, G. Bussi, A. Ruini, E. Molinari, M.J. Caldas, Phys. Rev. B **81**, 081202 (2010)
22. G. Kresse, M. Marsman, L.E. Hintzsche, E. Flage-Larsen, Phys. Rev. B **85**, 045205 (2012)
23. S.L. Adler, Phys. Rev. **126**, 413 (1962)
24. N. Wiser, Phys. Rev. **129**, 62 (1963)
25. M.S. Hybertsen, S.G. Louie, Phys. Rev. B **34**, 5390 (1986)
26. R.W. Godby, R. Needs, Phys. Rev. Lett. **62**, 1169 (1989)
27. D.L. Johnson, Phys. Rev. B **9**, 4475 (1974)
28. M. Giantomassi, M. Stankovski, R. Shaltaf, M. Grüning, F. Bruneval, P. Rinke, G.-M. Rignanese, Phys. Status Solidi B **248**, 275 (2011)
29. S. Lebègue, B. Arnaud, M. Alouani, P.E. Blöchl, Phys. Rev. B **67**, 155208 (2003)
30. X. Gonze et al., Comput. Phys. Commun. **180**, 2582 (2009)
31. N. Troullier, J.L. Martins, Phys Rev. B **43**, 1993 (1991)
32. M. Rohlfing, P. Krüger, J. Pollmann, Phys. Rev. B **57**, 6485 (1998)
33. J.P. Perdew, Y. Wang, Phys. Rev. B **45**, 13244 (1992)
34. K. Kihara, G. Donnay, Can. Mineral. **23**, 647 (1985)
35. H.J. Monkhorst, J.D. Pack, Phys. Rev. B **13**, 5188 (1976)
36. J. Haines, J.M. Léger, Phys. Rev. B **55**, 11144 (1997)
37. R.W.G. Wyckoff, *Crystal Structures* (Interscience, New York, 1963)
38. R. Shaltaf, G.-M. Rignanese, X. Gonze, F. Giustino, A. Pasquarello, Phys. Rev. Lett. **100**, 6401 (2008)
39. W. Kang, M. Hybertsen, Phys. Rev. B **82**, 085203 (2010)
40. L. Ley, R.A. Pollak, F.F. McFeely, S. Kowalczyk, D.A. Shirley, Phys. Rev. B **9**, 600 (1974)
41. J.-M. Themlin, M. Chtab, L. Henrard, P. Lambin, J. Darville, J.-M. Gilles, Phys. Rev. B **46**, 2460 (1992)
42. T. Nagata, O. Bierwagen, M.E. White, M.-Y. Tsai, J.S. Speck, J. Appl. Phys. **107**, 033707 (2010)
43. M. Oshikiri, F. Aryasetiawan, J. Phys. Soc. Jpn **69**, 2123 (2000)
44. S. Tsoi, X. Lu, A.K. Ramdas, H. Alawadhi, M. Grimsditch, M. Cardona, R. Lauck, Phys. Rev. B **74**, 165203 (2006)
45. M. Batzill, U. Diebold, Prog. Surf. Sci. **70**, 47 (2005)
46. H.R. Philipp, Solid State Commun. **4**, 73 (1966)
47. H.R. Philipp, J. Phys. Chem. Sol. **32**, 1935 (1971)
48. V.P. Zakaznova-Herzog, H.W. Nesbitt, G.M. Bancroft, J.S. Tse, X. Gao, W. Skinner, Phys. Rev. B **72**, 205113 (2005)
49. F. Bruneval, N. Vast, L. Reining, Phys. Rev. B **74**, 045102 (2006)